AIAA JOURNAL
Vol. 45, No. 7, July 2007

Mechanisms Influencing the Efficiency of Oscillating Airfoil Propulsion

John Young* and Joseph C. S. Lai†
University of New South Wales, Australian Defence Force Academy, Canberra, Australian Capital Territory 2600, Australia

DOI: 10.2514/1.27628

A NACA0012 airfoil undergoing pitching and plunging motion at $Re = 20,000$–$40,000$ was simulated using a two-dimensional Navier–Stokes flow solver. Results were compared with experimental measurements in the literature and those from an inviscid analytical method and an unsteady panel method code. Although the peak in propulsive efficiency with Strouhal number demonstrated in the experimental results was predicted by the inviscid methods, it was found to be significantly modified by leading-edge vortex shedding and viscous drag at low Strouhal numbers. The occurrence and influence of vortex shedding is controlled by both the motion of the airfoil (amplitudes and phases of plunging and pitching) and the flapping frequency, which limits the time available for vortex formation and convection over the airfoil surface. Thus, Strouhal number alone is insufficient to characterize the efficiency of flapping-foil propulsion.

Nomenclature

A	=	amplitude of the airfoil trailing-edge net vertical motion (peak to peak)
$C_{P\text{mean}}$	=	time-averaged coefficient of the power required to drive the airfoil motion
$C_{T\text{mean}}$	=	time-averaged coefficient of the thrust generated by the airfoil
c	=	airfoil chord
c_p	=	coefficient of pressure
f	=	oscillation frequency
h	=	plunge amplitude nondimensionalized by the airfoil chord
k	=	reduced frequency, $\pi fc/U_\infty$
Re	=	freestream Reynolds number
Sr	=	Strouhal number, fA/U_∞
T	=	plunge motion period, f^{-1}
t	=	time
U_∞	=	freestream velocity
$y(t)$	=	plunging motion, $hc\sin(2\pi ft)$
η	=	propulsive efficiency
$\theta(t)$	=	pitching motion, $\theta_0\sin(2\pi ft + \psi)$
θ_0	=	pitch amplitude
τ	=	nondimensional time, t/T
ψ	=	phase angle between the pitching and plunging motions

I. Introduction

OSCILLATING foils are being considered for propulsion of submersible vehicles and micro air vehicles (MAVs) at low Reynolds numbers (for which conventional propulsion techniques become inefficient). Several studies of flapping-wing and tail propulsion in nature [1,2] have shown a propensity for a wide variety of animals to cruise within a narrow band of Strouhal number (defined as $Sr = fA/U_\infty$, where f is the flapping frequency, U_∞ is the forward speed of the animal, and A is an amplitude of motion taken as the total excursion of the tail trailing edge or the wingtip). These studies have shown optimum propulsive efficiencies within an approximate range of $0.2 < Sr < 0.4$, and numerical studies [3,4] have shown similar results. There is, however, evidence to suggest that the Strouhal number alone is insufficient to characterize the aerodynamics/hydrodynamics of flapping-foil propulsion, particularly when significant leading- or trailing-edge separation is present [5–7].

The objective of this work is to use a 2-D unsteady Navier–Stokes (NS) solver [8,9] to explore the effect of flow separation on the thrust and efficiency of an airfoil undergoing various combinations of large-amplitude sinusoidal pitching and plunging motions. Comparisons are made with the inviscid flat-plate analysis of Garrick [10] and an unsteady inviscid panel method [8], to determine the source of any peak in efficiency as a function of the Strouhal number. The small-amplitude, high-frequency motions associated with aeroelastic and aeroacoustic phenomena are considered elsewhere [11,12].

II. Analytical and Numerical Methods

The unsteady flowfield around an oscillating airfoil is simulated using a second-order-accurate, 2-D, compressible Navier–Stokes solver at low Mach number ($M_\infty = 0.05$). The equations are solved on a structured C-grid wrapped around the airfoil. The method uses Crank–Nicolson second-order time discretization, viscous flux terms are evaluated using second-order central differences in space, and inviscid fluxes are evaluated with a third-order-accurate Osher upwind scheme. The resulting semi-implicit equations are solved using Newton subiteration. Motion of the airfoil is introduced by a combination of rigid-body motion and deformation of the grid. Details of the method and quantitative and qualitative validation against results in the literature can be found in Tuncer and Platzer [13,14], Ekaterinaris and Platzer [15], Tuncer et al. [16], Young [12], and Young and Lai [8]. Results presented here use a 541×61 grid (377 points around the airfoil surface, first normal grid point at 8.75×10^{-6} chord lengths from the surface, with $y^+ < 1.0$ for all runs conducted), boundaries at 20 chords from the airfoil, and nondimensional time step $U_\infty \Delta t/(cM_\infty) = 9.5 \times 10^{-4}$, for which the aerodynamic forces are grid- and time-step-independent. These parameters resulted in approximate time steps per flapping cycle of between 10,000 (for reduced frequency $k = 6.3$) and 330,000 (for $k = 0.2$).

To isolate elements of the controlling physics of the oscillating airfoil flow, comparison is made with the analysis of Garrick [10],

Received 3 September 2006; revision received 2 April 2007; accepted for publication 2 April 2007.

*Lecturer, School of Aerospace, Civil and Mechanical Engineering; j.young@adfa.edu.au. Member AIAA.
†Professor, School of Aerospace, Civil and Mechanical Engineering; j.lai@adfa.edu.au. Associate Fellow AIAA.

which assumes a flat-plate airfoil and small amplitudes of motion, places shed vorticity in the form of a continuous vortex sheet on the centerline of motion, and allows no evolution of the vortex sheet in response to self-induced velocities. An unsteady panel method (UPM) code has also been developed [8,12] following Basu and Hancock [17] and Jones et al. [18]. The method allows arbitrary airfoil shapes, assumes inviscid and incompressible flow, enforces the Kutta condition at the trailing edge, and does not allow any separation over the airfoil surface. As the airfoil translates and the lift changes, vorticity is shed into the wake at each time step as a series of discrete point vortices that are convected due to freestream and self-induced velocities, thus the nonlinear character of the wake is preserved. Validation of the method may be found in Young [12]. Results presented here use 400 panels around the airfoil and 200 Rankine vortices shed into the wake per flapping cycle.

To further evaluate the influence of the wake structure and evolution on the forces developed by the airfoil, the UPM code has been subdivided into three versions. The flat-wake model places all shed vortices on the motion centerline and allows no wake evolution (apart from convection due to the freestream velocity), in a manner similar to the Garrick [10] analysis, but allows arbitrary airfoil motions. The fixed-wake model sheds the vortices along the line of the trailing-edge motion, but still allows no wake evolution. The free-wake model sheds vortices from the trailing edge, and the wake is free to evolve. Comparison of Garrick and the various UPM model results will determine the role of wake dynamics in the generation of the aerodynamic forces on the airfoil. The UPM code cannot simulate viscosity or leading-edge shedding of vorticity, and so comparison with NS results will determine the importance of viscous and separation effects.

III. Thrust, Power, and Propulsive Efficiency

Two airfoil motions were considered: the first was pure plunging motion of a NACA0012 airfoil with amplitude $h = 0.175$ and reduced frequency in the range $k = 0.0$ to 6.3, at $Re = 20,000$, as studied by Heathcote et al. [19]. The second was combined pitching and plunging motion at $Re = 40,000$, with the constraint of constant $\alpha_0 = \theta_0 - \tan^{-1}(2kh)$ and the pitching pivot point at one-third chord, as studied by Anderson et al. [4]. Plunge amplitudes $h = 0.25$ and 0.75, reduced frequencies $k = 0.0$ to 2.15, pitch phases $\psi = 75$ and 90 deg, pitch amplitudes $\theta_0 = -15$ to 55 deg, and constraints $\alpha_0 = 5$ and 15 deg were considered. Outputs for all cases included the mean (i.e., time-averaged) thrust coefficient $C_{T\text{mean}}$, input power coefficient $C_{P\text{mean}}$, and propulsive efficiency:

$$C_{T\text{mean}} = -\frac{1}{T}\int_t^{t+T} C_D(t)\,\mathrm{d}t$$

$$C_{P\text{mean}} = -\frac{1}{T}\int_t^{t+T} [C_L(t)\dot{y}(t)/c + C_M(t)\dot{\theta}(t)]\,\mathrm{d}t$$

$$\eta = C_{T\text{mean}}/C_{P\text{mean}}$$

where C_D, C_L, and C_M are the drag, lift, and moment coefficients calculated by integrating viscous and pressure forces around the airfoil surface, with the moment measured about the pivot point.

Figure 1 shows a comparison of the pure plunging experimental thrust, power, and efficiency results of Heathcote et al. [19], with NS and UPM (free-wake) simulations and Garrick [10] analytical results, as a function of the Strouhal number (with amplitude taken to be $A = 2hc$). The flow for the NS solver was assumed to be fully laminar at this Reynolds number ($Re = 20,000$), in accord with the observations of Young and Lai [8] and Young [12]. The NS code very closely reproduces the mean thrust and mean power coefficient at all reduced frequencies, with very minor differences reflected in the slight overprediction of efficiency at intermediate efficiencies. The trend in the experimental efficiency is well matched by the NS code, with a peak close to the correct magnitude and frequency and very similar rapid dropoff at low frequencies and gradual dropoff at high frequencies. The Garrick [10] and UPM methods both overpredict the thrust and underpredict the power, resulting in

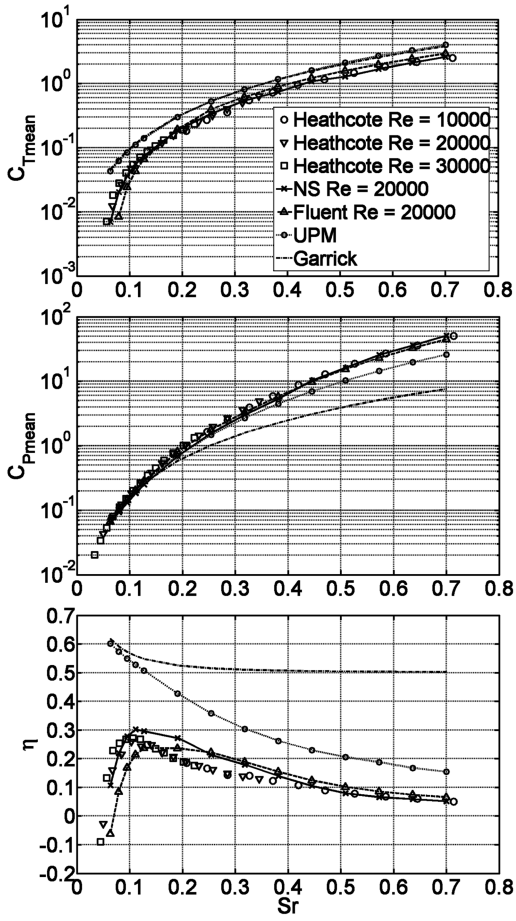

Fig. 1 Mean thrust coefficient, mean power coefficient, and propulsive efficiency; pure plunging motion ($h = 0.175$).

efficiencies that are much too high, although the UPM code does show a similar trend in the reduction of efficiency at higher frequencies. As additional validation of the NS results, the runs were repeated using the commercial CFD package Fluent version 6.2, with the incompressible solver, second-order upwind spatial discretizations, and pressure-velocity coupling via the SIMPLE algorithm. The Fluent runs used the same grid as for the NS runs as a core that moved as a rigid body, embedded within a deforming mesh of triangular cells, using the dynamic mesh feature; which limited time integration to first order. The flow was again assumed to be laminar. The thrust and power results are seen to be very similar to the NS results, with some difference in the location of the efficiency peak, but the trends are in very good agreement.

Figure 2 shows the combined pitching and plunging motion experimental thrust, power, and efficiency results of Anderson et al. [4] as a function of the Strouhal number (amplitude A taken to be the total vertical excursion of the airfoil trailing edge) for $h = 0.25$ and $\psi = 90$ deg, with θ_0 and k varying with the Strouhal number under the constraint $\alpha_0 = 15$ deg. Also shown are the corresponding NS results, with fully laminar and fully turbulent flow assumed (Baldwin–Lomax and Spalart–Allmaras turbulence models were used and produced very similar results; see Fig. 7.3 of Young [12]), as well as the UPM (free-wake) and Garrick [10] analysis results. The experimental results of Anderson et al. [4] show monotonically increasing thrust and power, with an increasing Strouhal number and a peak in propulsive efficiency in the range of $0.1 < Sr < 0.2$. The NS code shows good agreement with the experimental results in terms of the shape and location of the efficiency peak, at a Strouhal number of approximately $Sr = 0.16$, with little disagreement between laminar and turbulent results. Unlike the pure plunging case, both the Garrick [10] analysis and UPM (free-wake) results now predict an efficiency peak, although at a slightly lower Strouhal number than the NS and experimental results. The UPM code well

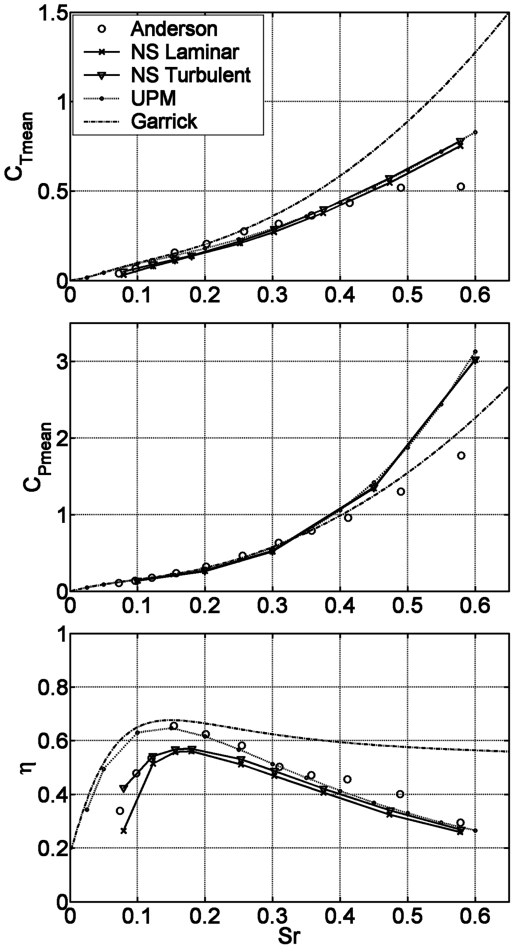

Fig. 2 Mean thrust coefficient, mean power coefficient, and propulsive efficiency; pitch and plunge motion ($h = 0.25$, $\psi = 90$ deg, $\alpha_0 = 15$ deg, and $Re = 40,000$).

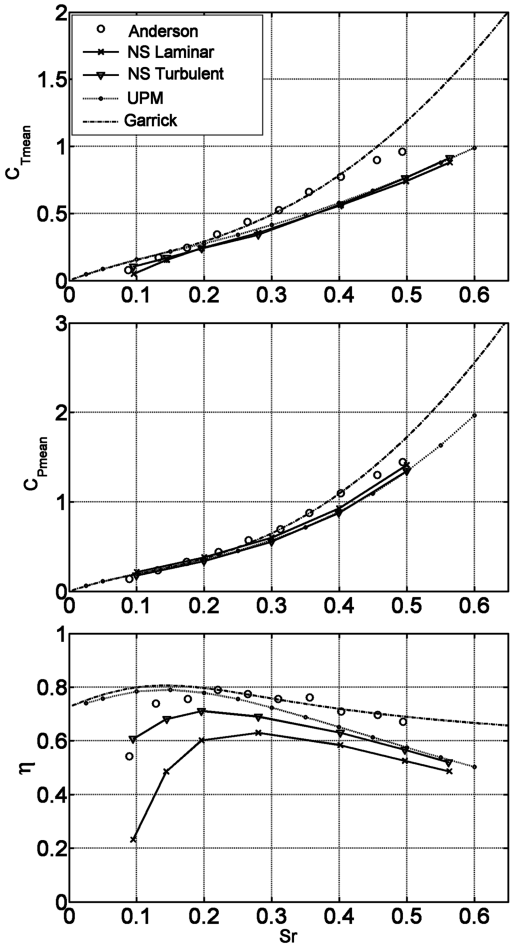

Fig. 3 Mean thrust coefficient, mean power coefficient, and propulsive efficiency; pitch and plunge motion ($h = 0.75$, $\psi = 90$ deg, $\alpha_0 = 15$ deg, and $Re = 40,000$).

captures the efficiency dropoff for $Sr > 0.16$, but overpredicts the efficiency at low Strouhal numbers. The Garrick analysis overpredicts the efficiency at all Strouhal numbers. Both NS and UPM mean thrust coefficient results closely follow the experimental results, except near $Sr = 0.6$, when the Anderson et al. [4] results show a leveling off in thrust. The Garrick [10] analysis predicts the thrust well at low Strouhal numbers, but overpredicts substantially at $Sr = 0.58$. The reverse is true for the mean power, for which the Garrick analysis correlates reasonably well with the experimental results and the NS and UPM results compare well at low Strouhal numbers, but overpredict by up to 70% at $Sr = 0.58$.

Figure 3 shows the same set of results, now with an increased plunge amplitude $h = 0.75$, but with unchanged phase $\psi = 90$ deg and $\alpha_0 = 15$ deg. The experiment again shows monotonic increases in mean thrust and power, but now produces higher efficiencies and a broader efficiency peak at higher Strouhal numbers somewhere in the range of $0.15 < Sr < 0.3$). The Garrick [10] analysis captures the thrust and power results reasonably well, whereas the UPM model matches the power, but underpredicts the thrust. The Garrick and UPM models predict an efficiency peak, but again at lower Strouhal numbers than the experimental results. The UPM code captures the slow reduction in efficiency at high Strouhal numbers but not the rapid reduction at low Strouhal number, whereas the Garrick analysis does not correctly predict either the high or low Strouhal number behavior. The NS simulations capture the power well but underpredict the thrust and experimental efficiency results, with the turbulent cases closer to experimental values than the laminar cases. However, the NS results well follow the form of the experimental efficiency variation with the Strouhal number, showing an efficiency peak in the same range of $0.15 < Sr < 0.3$ and capturing the reduction in efficiency outside this range.

Two other cases were considered ($h = 0.75$, $\psi = 75$ deg, and $\alpha_0 = 15$ deg and $h = 0.75$, $\psi = 90$ deg, and $\alpha_0 = 5$ deg) with similar levels of agreement between NS, UPM, Garrick [10], and experimental curves. Results are not presented here due to space limitations, but may be found in Young [12]. Overall for the Heathcote et al. [19] and Anderson et al. [4] cases, the NS results show good agreement with the experiment at all Strouhal numbers, the UPM results show reasonable agreement at higher Strouhal numbers, and the Garrick [10] efficiency results are poor at all Strouhal numbers. Comparison is now made between the three prediction techniques to determine the physical basis for the efficiency peak with Strouhal number.

IV. Origin of the Optimum Strouhal Number Range for High Propulsive Efficiency

A. Wake Dynamics

Taking the second Anderson et al. [4] case ($h = 0.75$, $\psi = 90$ deg, and $\alpha_0 = 15$ deg) as an example, Fig. 4 compares the results of the Garrick [10] analysis with the UPM free-wake, fixed-wake, and flat-wake models. The UPM flat-wake model shows thrust, power, and efficiency results very similar to the Garrick analysis, whereas the fixed-wake and free-wake results are almost identical to each other, but significantly different from the Garrick and flat-wake results. This indicates that at the oscillation frequencies considered for this case (approximately $0 < k < 1.1$), rollup of the shed vortex sheet into discrete vortices in response to the self-induced velocity field of the wake has a negligible effect on the aerodynamic forces and propulsive efficiency (similarity of free-wake and fixed-wake results). In contrast, as the Strouhal number is increased, the shedding of the vortex sheet at an increasingly large distance from the

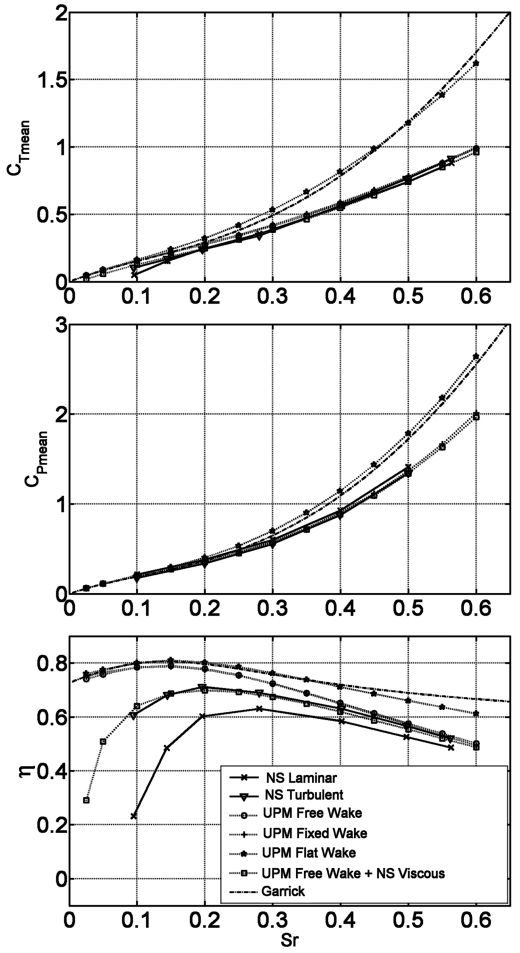

Fig. 4 Mean thrust coefficient, mean power coefficient, and propulsive efficiency; pitch and plunge motion ($h = 0.75$, $\psi = 90\,\text{deg}$, $\alpha_0 = 15\,\text{deg}$, and $Re = 40,000$).

motion centerline reduces the propulsive efficiency by significantly lowering the mean thrust produced (differences between fixed-wake and flat-wake results).

B. Viscous Effects

Also plotted in Fig. 4 are the UPM free-wake results, with the additional effect of the viscous forces estimated by subtracting the drag of the stationary airfoil from the UPM thrust. This drag contribution from the stationary airfoil is predicted by the NS code and includes both viscous friction and pressure drag due to separation at the trailing edge, but is hereafter referred to as *viscous drag*, for brevity. The viscous drag becomes a larger component of the total axial force on the airfoil as the Strouhal number is lowered, acting to lower the propulsive efficiency at low Strouhal numbers. This curve closely follows the NS turbulent results. However, the observed reduction is insufficient to explain the significant reduction in the NS efficiency as the Strouhal number is lowered for the laminar case, which is a better match for the shape of the efficiency curve in the experimental results.

C. Leading-Edge Vortex Shedding

In addition to being inviscid, the Garrick [10] and UPM models both apply the Kutta condition at the trailing edge to determine the total circulation on the airfoil. The flow is assumed to leave the trailing edge smoothly, and neither model can account for any flow separation anywhere on the airfoil surface. In contrast, the Navier–Stokes code simulates the boundary layer and can predict when local surface shear stress is reduced to zero and separation occurs. To quantify the effect of boundary-layer separation on the aerodynamic forces generated by the airfoil, surface-pressure-coefficient time

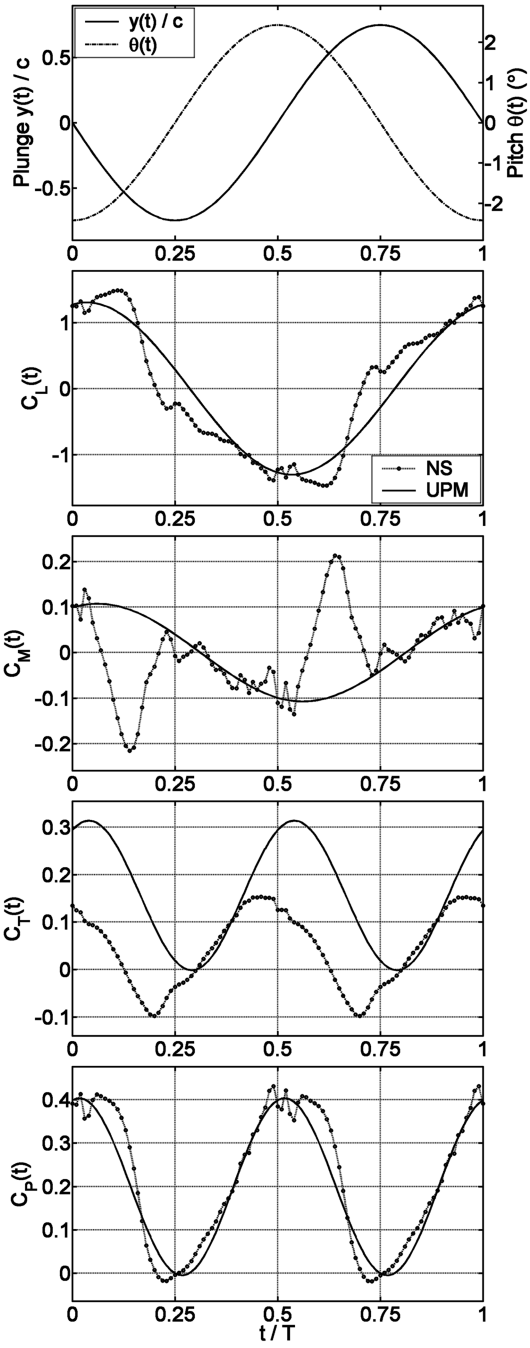

Fig. 5 Time histories of lift, moment, thrust, and power coefficients; Anderson et al. [4] motion $h = 0.75$; $\psi = 90\,\text{deg}$, $\alpha_0 = 15\,\text{deg}$, and $Sr = 0.1$; pressure forces only, viscous components ignored.

histories for UPM (free-wake) and NS (laminar) calculations are compared.

Figure 5 shows time histories of the lift, moment, thrust, and power coefficients for one flapping cycle at a low Strouhal number ($Sr = 0.1$, below the efficiency peak), with the motion corresponding to that considered in Fig. 3. The results shown are due solely to the surface pressure on the airfoil, and viscous forces are ignored to allow more direct comparison between the NS and UPM codes and to more clearly show the effect of flow separation. The NS lift coefficient roughly follows the UPM curve, but with oscillations about the underlying sinusoidal behavior. The NS moment coefficient also follows the UPM curve, with large deviations near cycle times $t/T = 0.125$ and $t/T = 0.625$ (with $t/T = 0$ corresponding to the pivot point at $y = 0$ and the airfoil moving downwards). The NS thrust coefficient is systematically lower than the UPM curve, with the greatest differences at $t/T = 0$ to 0.125 and

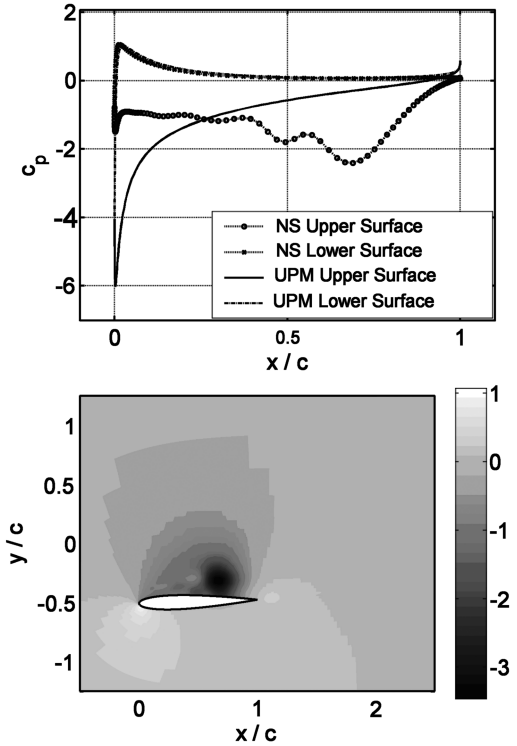

Fig. 6 Instantaneous pressure coefficient on the airfoil surface (NS laminar and UPM free wake, top) and in the surrounding flowfield (NS laminar, bottom); $Sr = 0.1$ and $t/T = 0.125$.

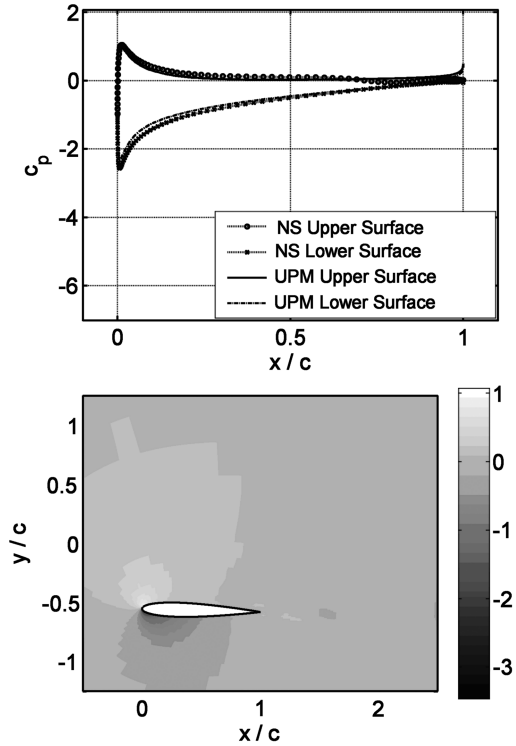

Fig. 7 Instantaneous pressure coefficient on the airfoil surface (NS laminar and UPM free wake, top) and in the surrounding flowfield (NS laminar, bottom); $Sr = 0.1$ and $t/T = 0.375$.

$t/T = 0.5$ to 0.625. The power-coefficient curves are quite similar, with some small deviations. Note that all the UPM and NS results are quite similar near $t/T = 0.375$.

Figures 6 and 7 show the pressure coefficient c_p on the surface of the airfoil (upper frames, NS and UPM results) and throughout the flowfield (lower frames, NS results) at the instants $t/T = 0.125$ and $t/T = 0.375$, respectively, in the flapping cycle for $Sr = 0.1$. Note that these figures are instantaneous, however, the flow is highly periodic and well established (i.e., transients have died down) and there is no discernible change in the pressure distribution at the same instant from flapping cycle to cycle. Here, a large vortex is seen to separate off the leading edge and is convected aft over the length of the airfoil. The vortex significantly alters the pressure distribution in comparison to the UPM results, as seen for $t/T = 0.125$ (causing the large deviations in the moment coefficient as it passes over the trailing edge). As the vortex forms, the associated low pressure contributes toward thrust as it acts on a section of the airfoil surface that is facing upstream and thus causes a forward suction. However, as the vortex is convected aft, it results in a drag force as it passes over the maximum thickness point of the airfoil, for which the airfoil surface now faces downstream and the vortex causes a rearward suction. Once the vortex has passed over the trailing edge into the wake, the NS and UPM surface-pressure distributions become very similar, as seen at $t/T = 0.375$. Overall, the time-averaged thrust coefficient is reduced over the complete flapping cycle, as seen in Fig. 5. The vortex contributes a locally increased lift on the airfoil compared with the UPM results, which opposes the plunging motion and so the contribution to input power is positive for the entire time the vortex stays over the airfoil surface. The net result of the thrust reduction and power increase is a large reduction in efficiency compared with the UPM results.

As the Strouhal number is increased (corresponding to greater pitching amplitude and greater reduced frequency), the occurrence and effect of leading-edge vortex shedding on the aerodynamic forces is lessened. Figures 8–10 show the same set of results as Figs. 5–7, but for $Sr = 0.5$ (above the efficiency peak). There is some evidence of vortex shedding off the leading edge and interaction of the vortices with the trailing edge (producing oscillations predominantly in the moment coefficient), but otherwise, the UPM and NS time histories closely follow each other.

As the oscillation reduced frequency increases with increasing Strouhal number, the period of the airfoil motion decreases. In contrast, the rate at which the flow can respond to a developing low-pressure suction peak by separating and forming a leading-edge vortex is fixed by the oncoming flow conditions. Also, the convection speed of the vortex aft over the airfoil stays relatively constant for the same reason. As the frequency increases, there is thus less time for the vortex to form and less time to travel downstream along the airfoil past the point of maximum thickness (when it contributes drag rather than thrust and lowers the propulsive efficiency) before the second half of the flapping cycle and a similar vortex on the opposite side of the airfoil.

Figures 11–13 again show the same set of NS and UPM results as for Figs. 5–7, now for the pure plunging motion of Heathcote et al. [19] ($h = 0.175$) for $Sr = 0.255$ (above the efficiency peak). When the stationary airfoil drag from the NS code is added to the UPM thrust for this case (shown in Fig. 14), the UPM efficiency drops off rapidly as the Strouhal number is lowered, but the reduction is again insufficient to explain the observed shape of the efficiency curve for the NS and experimental results. The Heathcote et al. motion shows an increasing tendency for leading-edge vortex shedding as the oscillation frequency rises and a relatively constant reduction in efficiency due to that vortex shedding. As may be seen in Figs. 11–13, the vortex that forms at or aft of the leading edge results in a much reduced suction pressure compared with the inviscid UPM code. This clearly reduces the thrust produced, but has very little effect on the lift, moment, and power required to drive the airfoil.

As a further test of the effect of the wake dynamics, viscous effects, and leading-edge flow separation, an attempt was made to remove any efficiency variation with the Strouhal number due solely to the motion. Figure 15 shows the propulsive efficiency predicted by the Garrick [10] analysis for a range of Strouhal numbers and pitch amplitudes. The plunge amplitude and the relative phase between pitch and plunge are chosen to be the same as for the motion depicted in Fig. 2; namely, $h = 0.25$ and $\psi = 90$ deg. Also shown are the combination of Strouhal number and θ_0 resulting from the Fig. 2

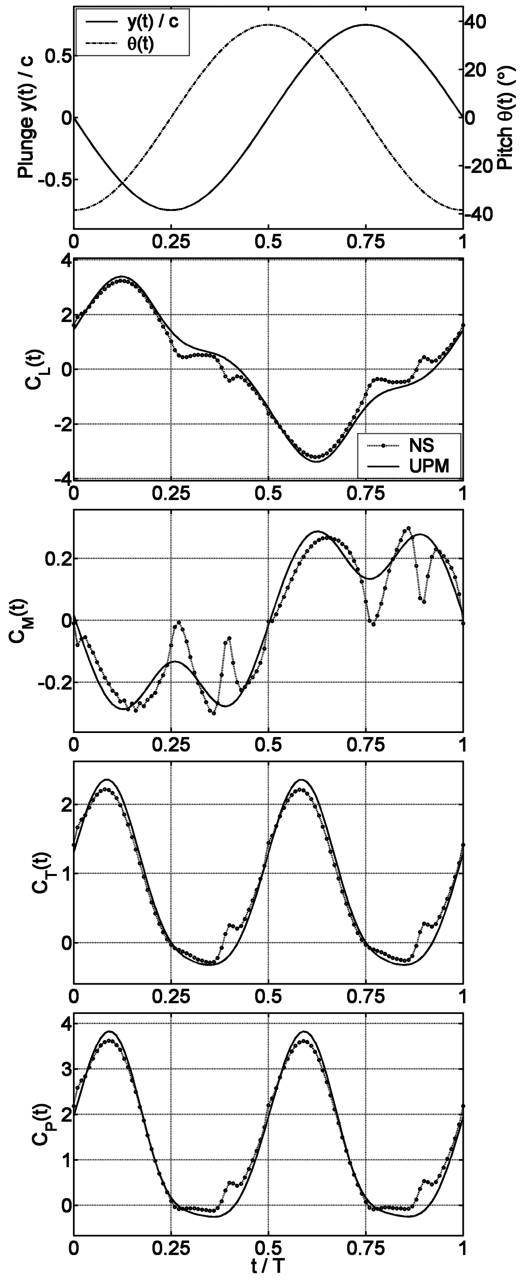

Fig. 8 Time histories of lift, moment, thrust, and power coefficients; Anderson et al. [4] motion $h = 0.75$; $\psi = 90\,\text{deg}$, $\alpha_0 = 15\,\text{deg}$, and $Sr = 0.5$; pressure forces only, viscous components ignored.

constraint $\alpha_0 = 15\,\text{deg}$, in accordance with the experiments of Anderson et al. [4]. The efficiency is plotted only for regions of the parameter space in which the mean thrust is positive. Note that at low Strouhal numbers, the θ_0 required (with given values of the flapping parameters h, ψ, and pivot point) to achieve that Strouhal number value can be negative.

The efficiency peak in the Fig. 2 Garrick [10] results is apparent in Fig. 15 as the Fig. 2 parameter curve crosses from a region of low efficiency over a "ridge" of higher efficiency then back down as the Strouhal number increases from 0.0 to 0.6. The efficiency peak is thus revealed as an artifact of the constraint chosen for the Fig. 2 runs (namely, that $\alpha_0 = 15\,\text{deg}$), rather than an inherent feature of the Garrick analysis itself. Quite clearly, any number of different selections of k and θ_0, still spanning the range of $0 < Sr < 0.6$ covered in Fig. 2 could be chosen that would result in a monotonic decrease in efficiency with Strouhal number.

Accordingly, a constant value of $\eta = 0.575$ was chosen, and the corresponding set of flapping parameters was simulated with the NS and UPM codes. The results are shown in Fig. 16. Even with the

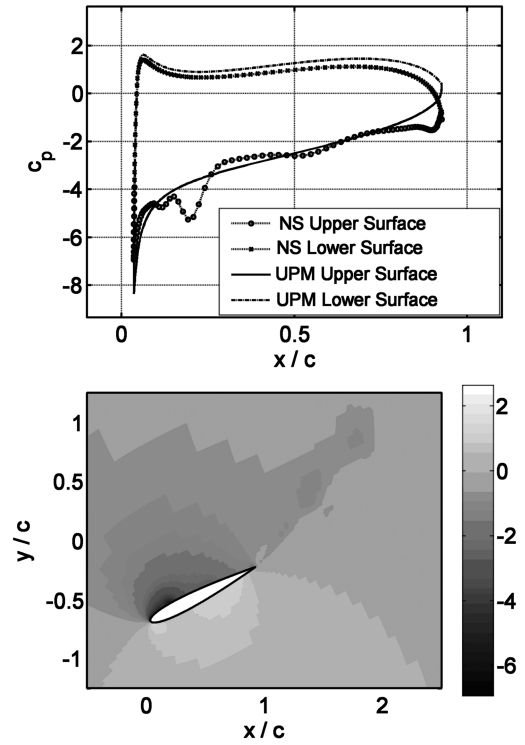

Fig. 9 Instantaneous pressure coefficient on the airfoil surface (NS laminar and UPM free wake, top) and in the surrounding flowfield (NS laminar, bottom); $Sr = 0.5$ and $t/T = 0.125$.

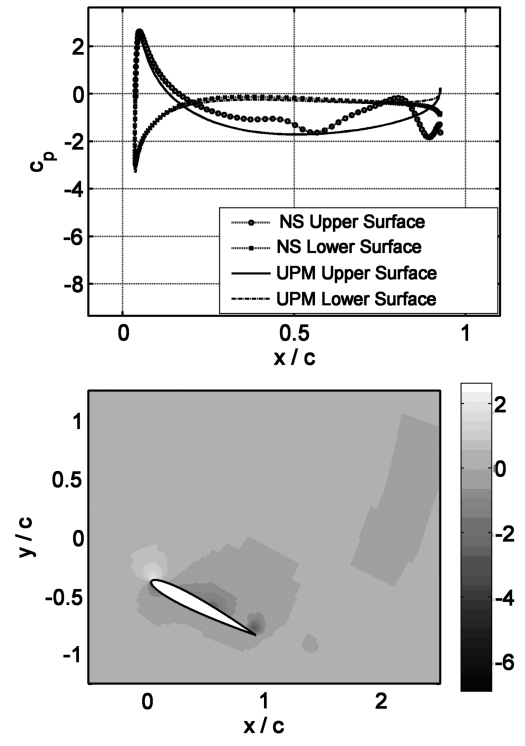

Fig. 10 Instantaneous pressure coefficient on the airfoil surface (NS laminar and UPM free wake, top) and in the surrounding flowfield (NS laminar, bottom); $Sr = 0.5$ and $t/T = 0.375$.

underlying efficiency peak removed from the Garrick [10] prediction, similar features to the Fig. 3 case are observed.

Now the NS code predicts a very broad efficiency peak somewhere in the range of $0.1 < \text{S}r < 0.4$. There is still negligible wake rollup (small differences between the fixed- and free-wake models) and a

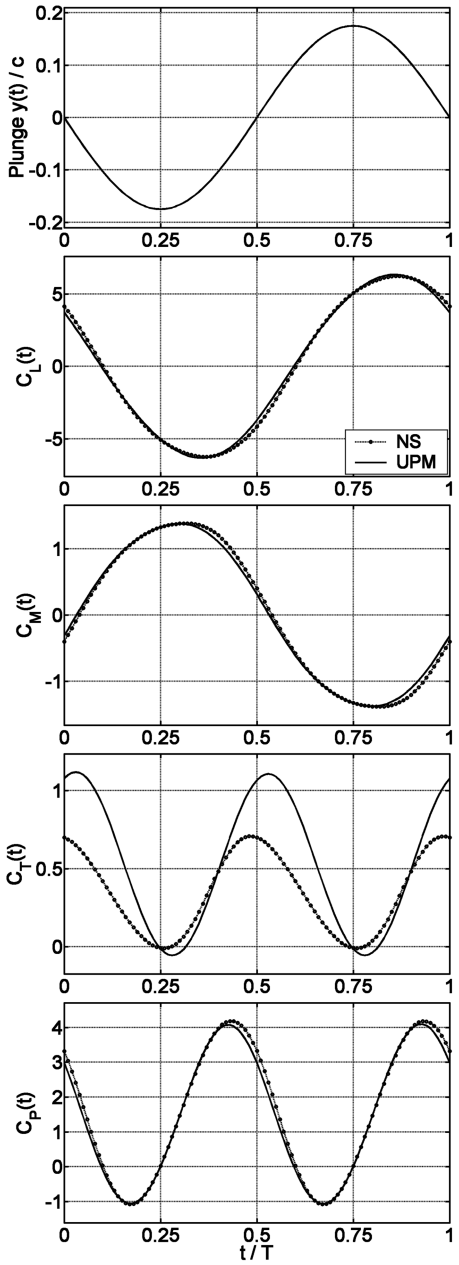

Fig. 11 Time histories of lift, moment, thrust, and power coefficients; Heathcote et al. [19] motion $h = 0.175$; $Sr = 0.255$; pressure forces only, viscous components ignored.

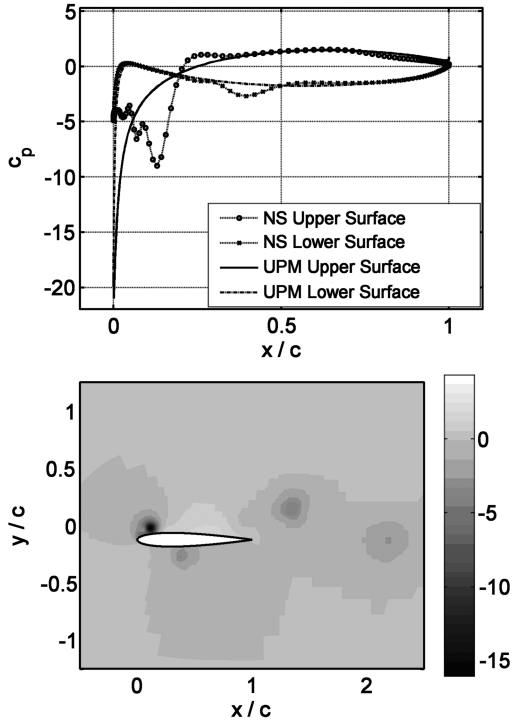

Fig. 12 Instantaneous pressure coefficient on the airfoil surface (NS laminar and UPM free wake, top) and in the surrounding flowfield (NS laminar, bottom); $Sr = 0.5$ and $t/T = 0.125$.

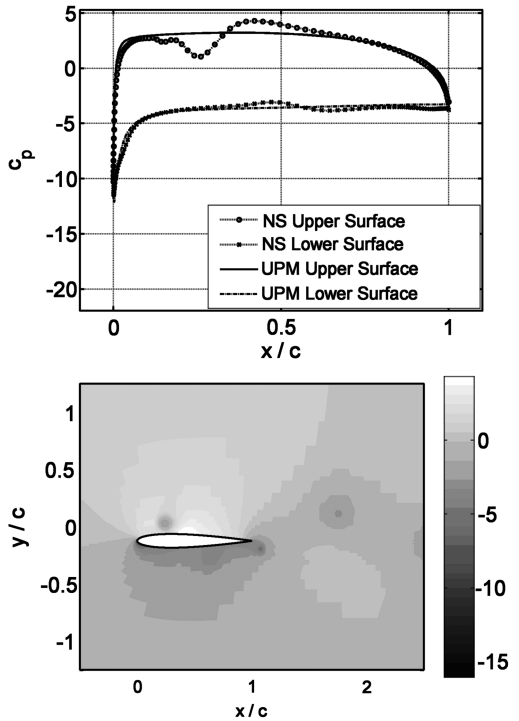

Fig. 13 Instantaneous pressure coefficient, on the airfoil surface (NS laminar and UPM free wake, top) and in the surrounding flowfield (NS laminar, bottom); $Sr = 0.5$ and $t/T = 0.375$.

reduction in efficiency at high Strouhal numbers due to a finite wake width (differences between the flat- and fixed-wake models). There is a sharp reduction in efficiency at low Strouhal numbers due to viscous drag, but this does not account for the remainder of the efficiency drop, which is again ascribed to leading-edge separation.

V. Conclusions

The peak in propulsive efficiency shown in the experiments of Anderson et al. [4] (combining pitch and plunge motions) is predicted with varying success by the small-amplitude, potential-flow, flat-plate Garrick [10] analysis. In contrast, the peak shown in the experiments of Heathcote et al. [19] (pure plunge motion) is not captured at all by the Garrick [10] analysis. Simulation with the unsteady panel method and NS codes indicates that the occurrence of a peak in propulsive efficiency, the magnitude of the peak, and the Strouhal number at which it occurs are all influenced by a number of physical mechanisms.

The wake becomes less "flat" as the Strouhal number is increased and vorticity is shed from the trailing edge further from the centerline of the flapping motion, which acts to reduce efficiency at high Strouhal numbers; leading-edge separation tends to reduce efficiency either at low Strouhal numbers or all Strouhal numbers, depending on the motion; viscous forces reduce efficiency at low Strouhal numbers; and self-induced rollup of the wake has little effect on the forces and propulsive efficiency at the frequencies considered here.

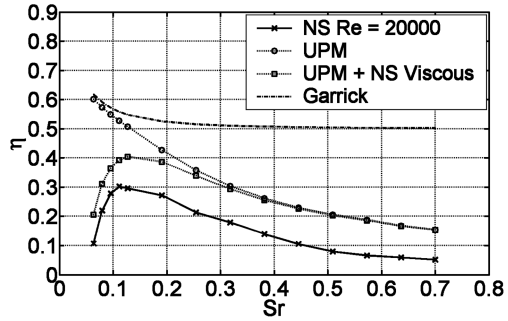

Fig. 14 Propulsive efficiency, Heathcote et al. [19] motion $h = 0.175$, NS laminar, UPM free wake, UPM free wake with viscous effects estimated from the NS simulations, and flat-plate analysis (Garrick [10]).

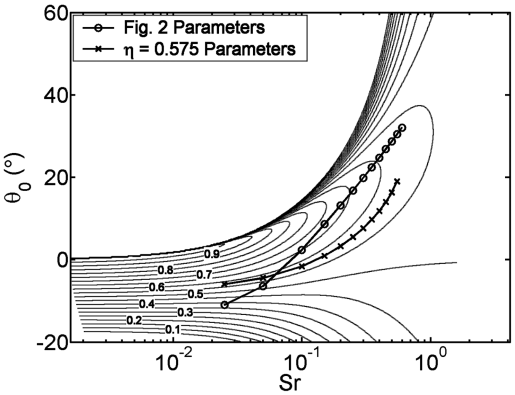

Fig. 15 Contours of propulsive efficiency; Garrick [10] analysis with $h = 0.25$; $\psi = 90\,\mathrm{deg}$; flapping parameters used in Fig. 2 that satisfy $\alpha_0 = 15\,\mathrm{deg}$ and parameters used in Fig. 16 that give constant $\eta = 0.575$.

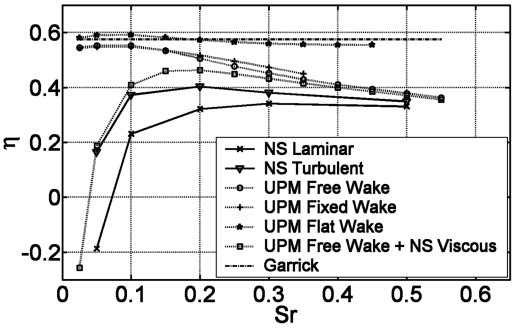

Fig. 16 Propulsive efficiency; pitch and plunge motion ($h = 0.25$, $\psi = 90\,\mathrm{deg}$, and $Re = 40,000$); θ_0 chosen as a function of the Strouhal number to give constant $\eta = 0.575$.

Flow separation and leading-edge shedding effects appear to be controlled by the reduced frequency by limiting the time available both for vortex formation and convection of the vortex over the airfoil surface. Also, the turbulence model used in the NS simulations has an influence on the details of the flow separation, but has a much smaller impact on the thrust than on the efficiency.

The overall effect of these phenomena is that an efficiency peak naturally emerges somewhere in the range of $0.1 < Sr < 0.4$. Any peak predicted by the inviscid flat-plate analysis is made sharper (that is, narrower, peaking across a smaller Strouhal number range) and moved toward a higher Strouhal number as a result of leading-edge vortex shedding and viscous drag. The magnitude, width, and location of the peak is highly dependent on the type of motion considered, as shown by the considerable variations between pure plunging and the various combined pitch and plunge motions considered here; thus, Strouhal number alone is insufficient to characterize the efficiency of flapping-foil propulsion. Note that due to the limited range of frequencies and amplitudes covered in this work, further experimental and computational investigation is required to draw general conclusions about the flow phenomena governing the most efficient flapping flight.

References

[1] Taylor, G. K., Nudds, R. L., and Thomas, A. L. R., "Flying and Swimming Animals Cruise at a Strouhal Number Tuned for High Power Efficiency," *Nature (London)*, Vol. 425, Oct. 2003, pp. 707–711.

[2] Triantafyllou, M. S., Triantafyllou, G. S., and Gopalkrishnan, R., "Wake Mechanics for Thrust Generation in Oscillating Foils," *Physics of Fluids A*, Vol. 3, No. 12, 1991, pp. 2835–2837.

[3] Read, D. A., Hover, F. S., and Triantafyllou, M. S., "Forces on Oscillating Foils for Propulsion and Maneuvering," *Journal of Fluids and Structures*, Vol. 17, Jan. 2003, pp. 163–183.

[4] Anderson, J. M., Streitlien, K., Barrett, D. S., and Triantafyllou, M. S., "Oscillating Foils of High Propulsive Efficiency," *Journal of Fluid Mechanics*, Vol. 360, Apr. 1998, pp. 41–72.

[5] Bandyopadhyay, P. R., Castano, J. M., Nedderman, W. H., and Donnelly, M. J., "Experimental Simulation of Fish-Inspired Unsteady Vortex Dynamics on a Rigid Cylinder," *Journal of Fluids Engineering*, Vol. 122, No. 2, 2000, pp. 219–238.

[6] Triantafyllou, M. S., Triantafyllou, G. S., and Yue, D. K. P., "Hydrodynamics of Fishlike Swimming," *Annual Review of Fluid Mechanics*, Vol. 32, 2000, pp. 33–53.

[7] Wang, Z. J., "Vortex Shedding and Frequency Selection in Flapping Flight," *Journal of Fluid Mechanics*, Vol. 410, May 2000, pp. 323–341.

[8] Young, J., and Lai, J. C. S., "Oscillation Frequency and Amplitude Effects on the Wake of a Plunging Airfoil," *AIAA Journal*, Vol. 42, No. 10, 2004, pp. 2042–2052.

[9] Young, J., Lai, J. C. S., Kaya, M., and Tuncer, I. H., "Thrust and Efficiency of Propulsion by Oscillating Foils," in *Computational Fluid Dynamics 2004*, edited by C. Groth and D. W. Zingg, Springer, Berlin, 2004, pp. 313–318.

[10] Garrick, I. E., "Propulsion of a Flapping and Oscillating Airfoil," NACA Rept. 567, May 1936.

[11] Young, J., and Lai, J. C. S., "Vortex Lock-In Phenomenon in the Wake of a Plunging Airfoil," *AIAA Journal*, Vol. 45, No. 2, 2007, pp. 485–490.

[12] Young, J., "Numerical Simulation of the Unsteady Aerodynamics of Flapping Airfoils," Ph.D. Thesis, School of Aerospace, Civil and Mechanical Engineering, Univ. of New South Wales, Canberra, Australia, 2005.

[13] Tuncer, I. H., and Platzer, M. F., "Thrust Generation Due to Airfoil Flapping," *AIAA Journal*, Vol. 34, No. 2, 1996, pp. 324–331.

[14] Tuncer, I. H., and Platzer, M. F., "Computational Study of Flapping Airfoil Aerodynamics," *Journal of Aircraft*, Vol. 37, No. 3, 2000, pp. 514–520.

[15] Ekaterinaris, J. A., and Platzer, M. F., "Computational Prediction of Airfoil Dynamic Stall," *Progress in Aerospace Sciences*, Vol. 33, Nos. 11–12, Apr. 1998, pp. 759–846.

[16] Tuncer, I. H., Walz, R., and Platzer, M. F., "A Computational Study on the Dynamic Stall of a Flapping Airfoil," 16th Applied Aerodynamics Conference, Albuquerque, NM, AIAA Paper 98-2519, 1998.

[17] Basu, B. C., and Hancock, G. J., "The Unsteady Motion of a Two-Dimensional Aerofoil in Incompressible Inviscid Flow," *Journal of Fluid Mechanics*, Vol. 87, No. 1, 1978, pp. 159–178.

[18] Jones, K. D., Dohring, C. M., and Platzer, M. F., "Wake Structures Behind Plunging Airfoils: A Comparison of Numerical and Experimental Results," 34th Aerospace Sciences Meeting and Exhibit, Reno, NV, AIAA Paper 96-0078, 1996.

[19] Heathcote, S., Wang, Z. J., and Gursul, I., "Effect of Spanwise Flexibility on Flapping Wing Propulsion," 36th AIAA Fluid Dynamics Conference and Exhibit, San Francisco, CA, AIAA Paper 2006-2870, 2006.

A. Plotkin
Associate Editor